LASER INTERFEROMETER GRAVITATIONAL WAVE OBSERVATORY
– LIGO –

LIGO Laboratory / LIGO Scientific Collaboration

𝕸𝖎𝖉𝖉𝖑𝖊 𝕷𝕴𝕲𝕺

P Fritschel, R Adhikari, R Weiss

Distribution of this draft:

This is an internal working note
of the LIGO Project.

California Institute of Technology
LIGO Project - MS 51-33
Pasadena CA 91125
Phone (626) 395-2129
Fax (626) 304-9834
E-mail: info@ligo.caltech.edu

Massachusetts Institute of Technology
LIGO Project - NW17-161
Cambridge, MA 01239
Phone (617) 253-4824
Fax (617) 253-7014
E-mail: info@ligo.mit.edu

LIGO Hanford Observatory
P.O. Box 1970
Mail Stop S9-02
Richland, WA 99352
Phone 509-372-8106
Fax 509-372-8137

LIGO Livingston Observatory
P.O. Box 940
Livingston, LA 70754
Phone 225-686-3100
Fax 225-686-7189

http://www.ligo.caltech.edu/

1 OVERVIEW

This document presents potential technical improvements to the initial LIGO Detectors. These improvements are targeted for implementation in the interval between the end of the S5 Science Run and the start of the Advanced LIGO hardware installation, and are intended to provide a significant sensitivity improvement over S5. As much as possible, the improvements employ technologies or techniques that are part of the Advanced LIGO design. This strategy not only takes advantage of Advanced LIGO R&D, but also is intended to make transitional steps towards Advanced LIGO. The benefits of transitioning towards Advanced LIGO are several: gaining more confidence that there are no unforeseen noise source or other limiting phenomena that lie between the initial and advanced sensitivities, or learning to deal with any that are discovered; early implementation and debugging of Advanced LIGO hardware on a full-scale interferometer, to reduce commissioning time of Advanced LIGO; gaining experience with higher power operation of a full-scale interferometer and its components, likely also to reduce commissioning time of AdLIGO.

The principal proposed improvement is an increase in laser power, aimed at improving the strain sensitivity around the minimum noise frequency by a factor of 2-2.5. The number of galaxies probed by the detectors would increase approximately 10 times. This paper describes the detector component and subsystem upgrades needed to achieve the power increase, the most complex of which is an in-vacuum output mode cleaner and anti-symmetric port detection system. Other potential improvements are also explored, involving a combination of low-frequency noise reduction measures, stability improvements, and implementations of Advanced LIGO technology. A conceptual plan for the schedule and cost estimates are presented for the various improvements.

2 TIMELINE

The S5 Science Run is intended to collect one year's worth of coincident data at design sensitivity. The run will start near the end of 2005, and is expected to last approximately 18 months. At the other end of the planning timeline, Advanced LIGO will hopefully be funded starting in FY2008 (fall of 2007). The first interferometer could be decommissioned for installation of AdLIGO hardware at the end of 2010. As shown in the timeline in Fig. 1, this leaves approximately 3½ years of additional operation of the initial LIGO interferometers, beyond S5. This is the time available for making improvements, beginning implementation of select Advanced LIGO technologies, and carrying out additional science runs with improved sensitivity.
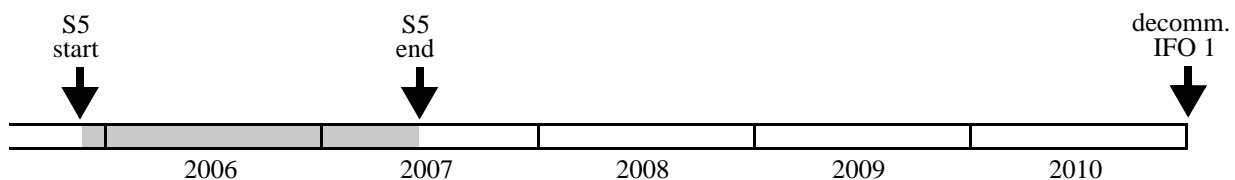

Figure 1: Timeline for LIGO detector operation over the next 5 years. It is anticipated that there will be approximately 3½ years between the end of S5 and the beginning of Advanced LIGO installation; this is time period for making detector improvements and carrying out additional science runs.

Any performance improvement steps must of course leave time for taking advantage of them with science mode running. A suggested approach is to plan for another 1½ year science run, ending at the point where the first interferometer is decommissioned for Advanced LIGO installation. This would leave approximately 2 years to implement and debug the interferometer improvements.

3   NOISE BUDGETS: CURRENT & FUTURE

In Fig. 2 below we show an H1 noise budget from fall 2005, which should be a good representation of the interferometer performance at the beginning of S5. In Fig. 3, we show the fundamental noise sources for the post-S5 interferometer improvements that are the subject of this paper.
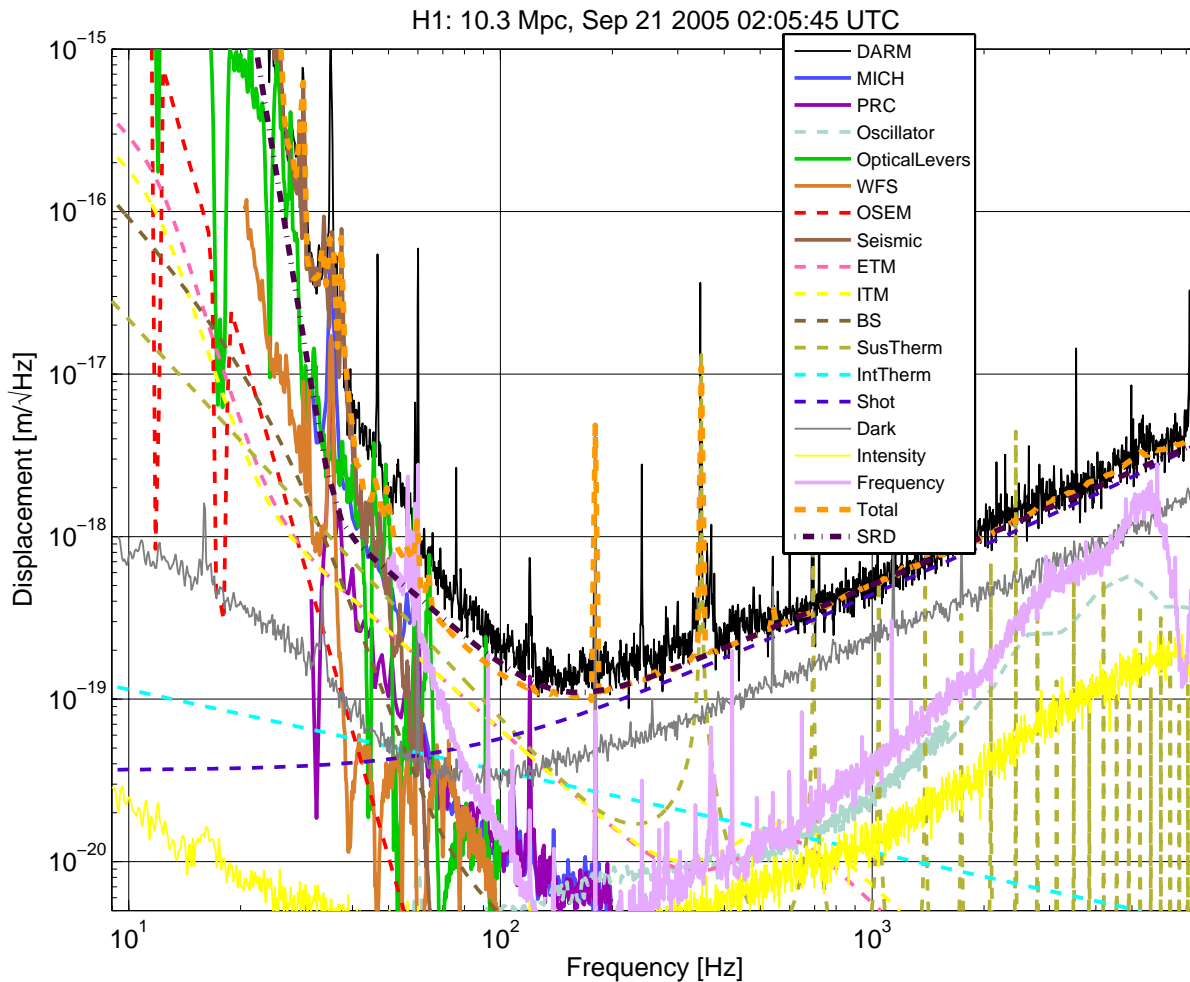

Figure 2: Noise budget for the H1 interferometer, at close to the maximum sensitivity seen at the end of September 2005. The laser power incident on the mode cleaner was 7.2 W, for an estimated power incident on the recycling mirror of 5 W. The noise budget does not fully explain the measured noise in the 40-100 Hz band. The excess noise may be upconversion from low frequency motion, possibly due to scattered light.

In xxx below we show an H1 noise budget from fall 2005, which should be a good representation of the interferometer performance at the beginning of S5.
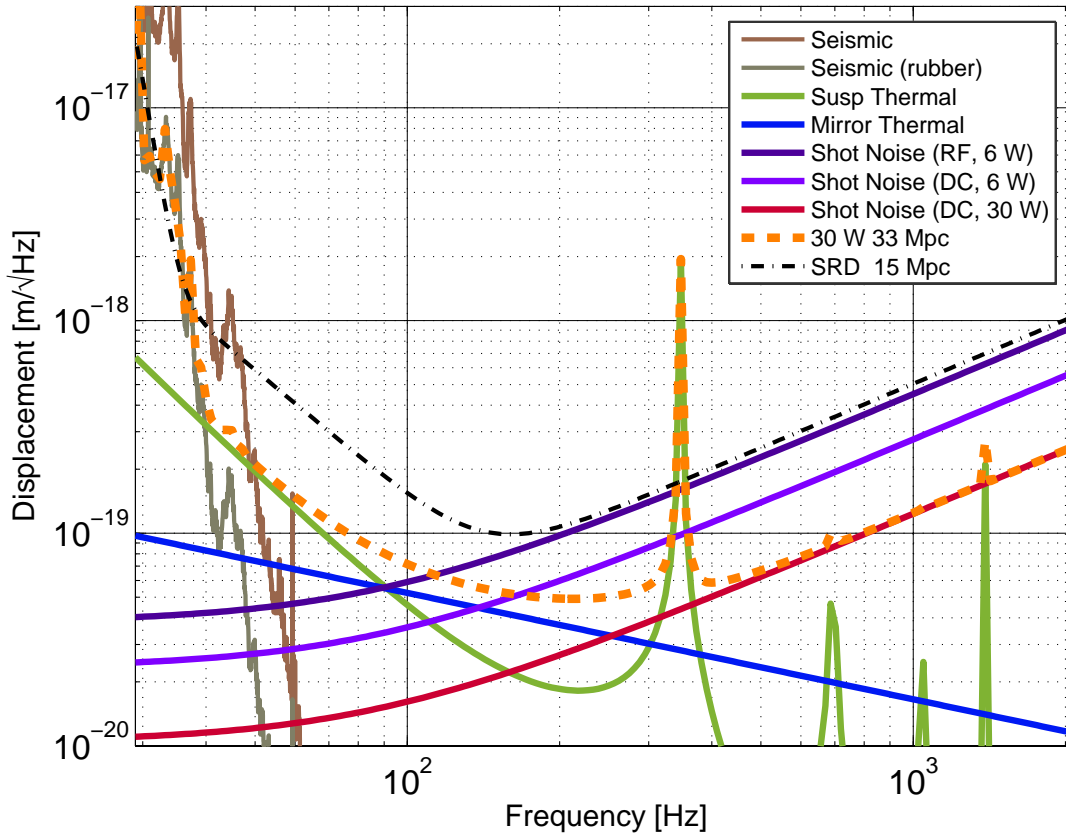

Figure 3: Fundamental noise sources for a set of middle LIGO options. The distances given for the last 2 curves (33.2 Mpc, 15 Mpc) are the standard range figures for NS/NS inspirals. The curves are calculated as follows. *Seismic:* LHO seismic noise, measured with the accelerometers mounted on the stack supports tubes, propagated through the Hytec stack model. *Seismic (rubber):* same as previous, with the addition of a low-pass filter, made by introducing an elastomer between the peir top and the stack support tube; this elastomer-filter is assumed to have an eigenfrequency of 9 Hz, a 10 dB peak amplfication, and $1/f$ filtering above that. *Steel (d = -1 cm):* suspension thermal noise from the current wire loop suspensions, assuming a wire structure damping of 3×10^{-4} and including thermoelastic damping; the cavity laser mode is positioned about 1 cm below the center of the optic, to minimize the noise below ~100 Hz. *Mirror thermal:* uses the mirror thermal noise formula from A. Gretarsson's Ph.D. thesis, with a bulk loss of 10^{-7} and a coating loss of 2×10^{-4}. *Shot Noise:* As described in detail in later sections, the shot noise contributions are compared for a few cases: RF v. DC readout and also for increasing the laser power into the interferometer to go from 6 W to 30 W into the RM. *30 W:* this is the sum of the curves 'seismic (rubber)', 'steel', 'mirror thermal', and 'shot noise (DC, 30 W)'; and it represents the goal noise spectrum for middle LIGO. Many technical noises would need to be reduced to approach this level; these are discussed in App. A. Possibilities for further reducing the suspension thermal noise are discussed in Sec. 8.2.

4   ASTROPHYSICS IMPACT

The impact of the various improvements that are described in this document on the sensitivity to gravitational wave (GW) sources is shown in Fig. 4 and Fig. 5. For a more detailed look at the detectability of periodic sources, see the recent article by B. Owen [1]; he concludes that a factor of 2 improvement in strain sensitivity below 200 Hz "would substantially improve the astrophysics reach of a broadband interferometer, even accounting for eighteen months downtime." In fact this would be true for all types of searches: a 1½ year science run at factor of 2 improved strain
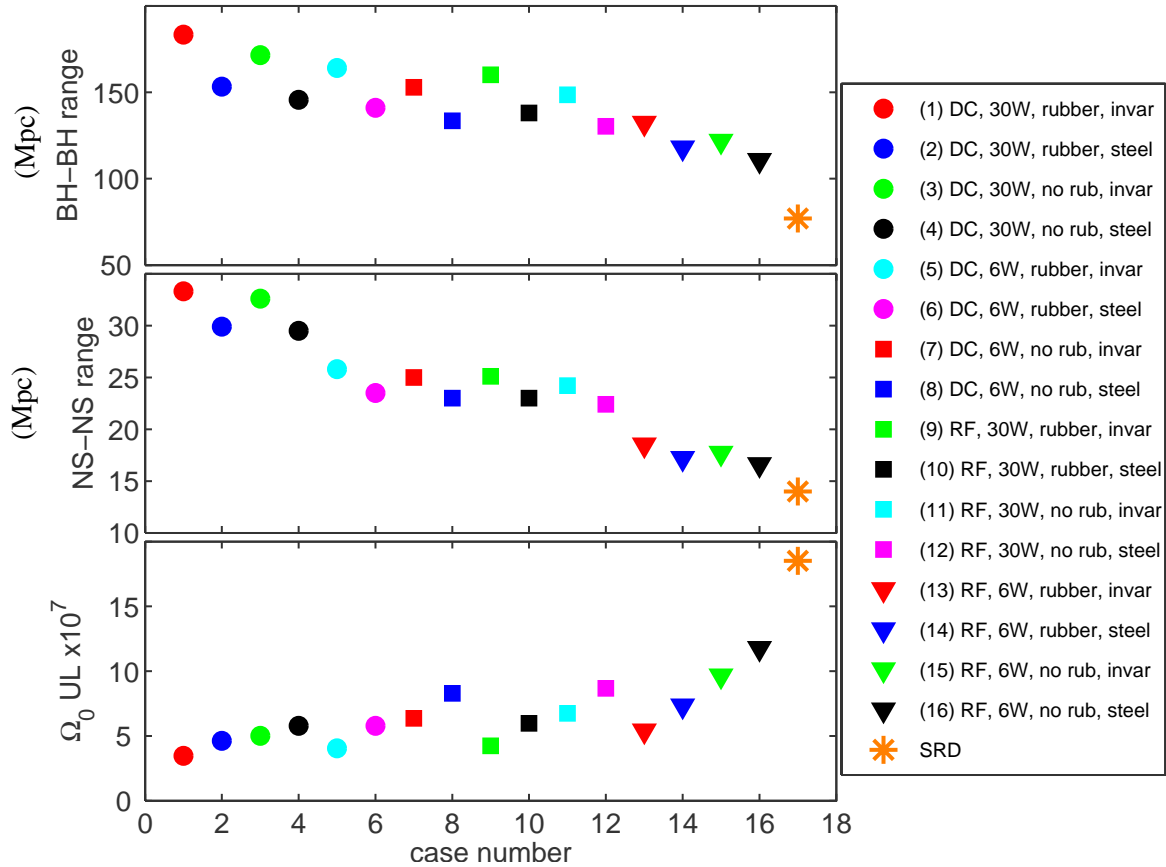

Figure 4: Sensitivity of various detector improvement combinations to several GW sources: black hole-black hole (BH-BH) binary inspirals, for 20 solar-mass BH pairs; 1.4 solar-mass neutron star (NS) binary inspirals; a stochastic background (Ω_0) with a constant energy density per logarithmic frequency interval. For the inspirals, the range is distance at which a single interferometer could detect the source with a SNR of 8, averaged over sky position and source polarization. For the stochastic background, the sensitivity is the upper limit that could be set, at 90% confidence, by correlating the LHO and LLO 4km interferometers, for a Hubble constant of 72 km/sec/Mpc. The case descriptors are: 'DC/RF', for DC or RF readout, both cases with an output mode cleaner; the power level is that at the input to the recycling mirror; 'rubber/no rub', referring to the additional passive seismic isolation described in Sec. 6.2.; 'invar/steel' for the suspension thermal noise model–'steel' is for the existing steel wire, and 'invar' simply assumes the thermal noise is sqrt(2)× lower than this, at all frequencies.

sensitivity would be more fruitful than a 3 year run at the S5/SRD sensitivity. For inspirals, recent population modeling [2] has shown that the number of Milky-Way equivalent galaxies (MWEG) probed by the detectors scales nearly as the cube of the detector range. A factor of 2 range

increase would thus open up approximately 8× more galaxies (going approximately from 400 to 3000 MWEG for NS-NS inspirals).
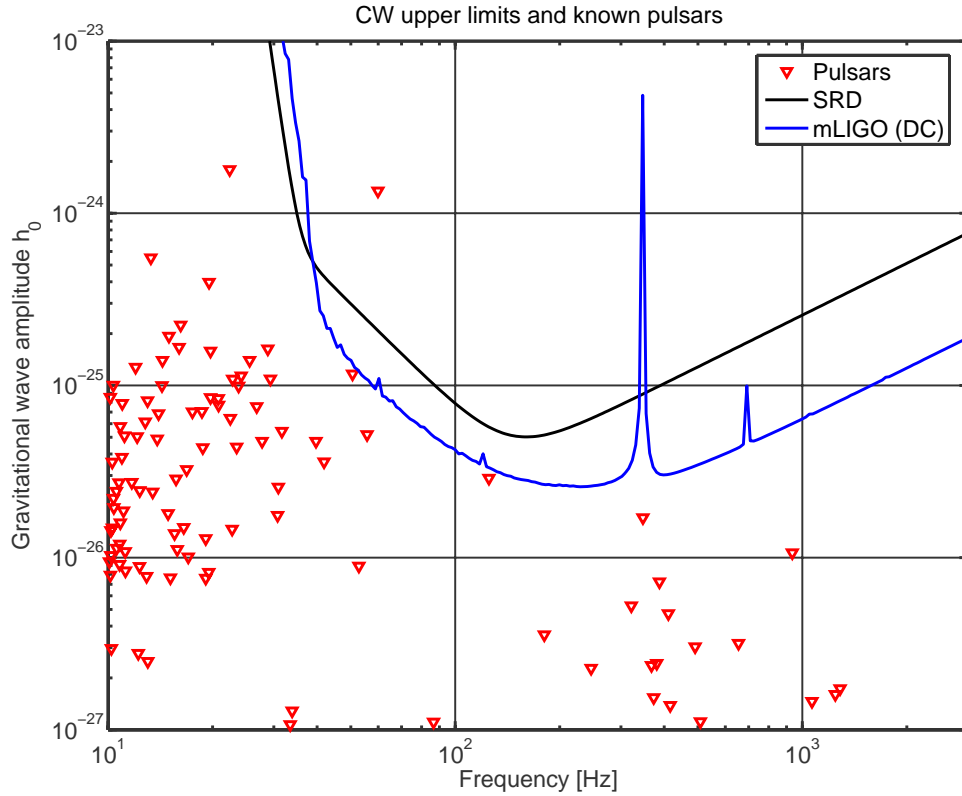

Figure 5: Sensitivity of initial and middle LIGO to known pulsars, for 1 year of data. The pulsar amplitudes are the spin-down limits; i.e., the GW strain amplitude if the pulsar frequency change were due entirely to GW emission. The blue curve is the same as the orange curve in Fig. 3; it shows marginal sensitivity to 2 additional known pulsars, and a factor of 2 more sensitive probing of the Crab pulsar.

5   HIGHER POWER

The goal of the laser power upgrade is to increase the stored power in the arms by a factor of 5 and achieve the corresponding sensitivity improvement. This requires: more laser power; new input optics components suitable for the higher power; an output mode cleaner and in-vacuum anti-symmetric port detection; thermal compensation.

5.1. Laser

Several options have been considered for a laser that could provide 40-50 W of power:

- some sort of early version of the Advanced LIGO laser from LZH (Laser Zentrum Hannover)
- an additional, higher-power amplifier head from Lightwave Electronics (now part of JDS Uniphase)

- other commercial amplifier heads

The second option turns out not to be viable. While LWE/JDSU certainly has the technology to produce a '40 W engine', there is no current product like this, and there is no intention to develop one (their products at this power level are pulsed devices). Regarding the third option, Cutting Edge Optronics (a division of Northrop Grumman) has a line of CW diode-pumped laser heads at medium- and high-power levels [3]. These are principally intended for industrial multi-mode laser applications, and it is unclear how efficient they would be at amplifying a TEM00 beam. They deserve a closer look.

LZH proposed two concepts at the March 2005 LSC meeting (LIGO-G050161-00). Both designs are amplifiers for the existing 10W LWE lasers; one is a multi-passed Nd:YAG rod, and the other is a single-pass, Nd:YVO, 4 rod amplifier. The latter design appears to be the simpler, and more capable system, and is diagrammed in Fig. 6. LZH's simulation of this system, based on measured single-rod gain measurements, predicts an output power of 45 W, for a 4-rod system and an input beam power of 10 W.
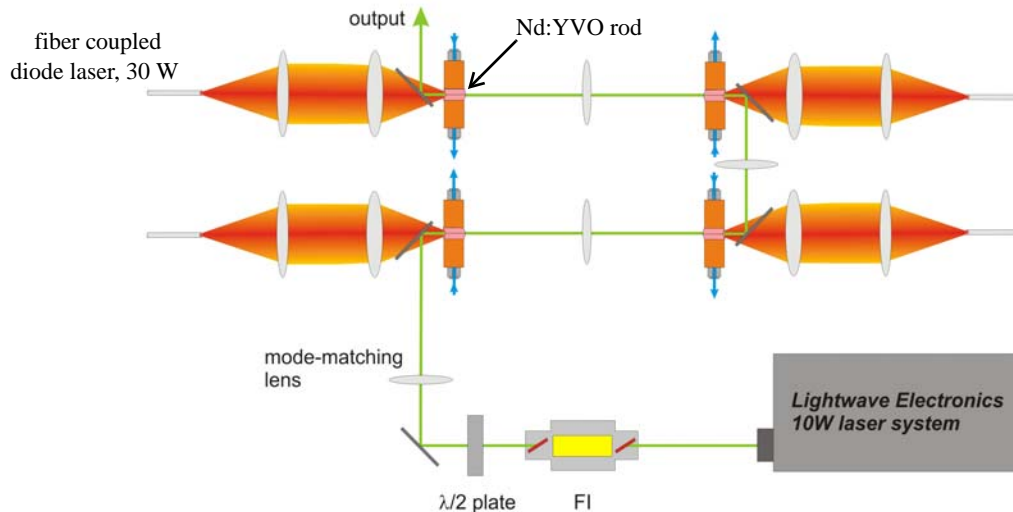

Figure 6: LZH amplifier concept based on 4 rods of Nd:YVO, each single-passed. The predicted output power of the above system is 45 W.

It is worth mentioning one more option, that is more limited in power but should be relatively inexpensive. That is to use the amplifiers from the existing JDSU/LWE MOPAs to amplify the 10W output from another JDSU MOPA. Such a system has been implemented at Stanford for several years, and it can yield approximately 30 W. There are 10 JDSU amplifiers within LIGO (including 2 units at Stanford, and one unit each at LASTI and the 40m), so it would be possible to outfit 3 interferometers with 2 amplifiers each, though with few spares. This path would require finding a substitute laser diode bar that could be retrofitted into the JDSU amplifiers.

Connection with Advanced LIGO. LZH is not prepared to deliver an early version of the Advanced LIGO laser (e.g., a scaled down version) in mid-2007, and so they proposed the alternative designs just discussed. Either of these designs would be developed by a different team than

the one working on the AdL laser, and wouldn't detract from that effort. The fiber-coupled diode pump lasers are a common design element with the AdL laser, and so there is the benefit of gaining early experience with the pumps. It is also worth noting that commissioning of the AdL interferometers could progress a very long way with such a 45 W laser source, and so having it installed and commissioned when AdL begins would thus reduce some of the early AdL commissioning work. Even though the amplifier is not in the baseline design of the AdL laser, developing it could have other benefits:

- the amplifier could replace the medium-power (12 W) injection-locked oscillator stage in the AdL, as the front end for the high-power injection-locked oscillator
- the amplifier could replace the current LWE (now JDSU) amplifiers, if these amplifiers degrade pass the point of usefulness and are no longer supported by JDSU

5.2. Input Optics

5.2.1.   Electro-optic modulators

The current LIGO LiNbO3 Electro-Optic Modulator (EOM) is only rated for use at ~10 W of power, and in fact damage has been seen in some of these units. Even if there were no damage at higher power, thermal lensing would become problematic. The high-power modulator being developed by the University of Florida group for AdLIGO uses RTP or RTA as the crystal, both of which can handle the AdLIGO power level with very little lensing. We thus propose to implement the AdL EOM design for middle-LIGO.

The R&D on the modulator material is sufficiently advanced for this purpose. The crystals have handled 95 W in the 300 micron beam, continuously for 400 hours. Piezo-resonances are exhibited above a few hundred kHz, similar to the current EOMs. The remaining work is the mounting and packaging of the modulator, for which two options have been suggested: contract with New Focus to package them, similar to the fashion they package the lithium niobate modulators; do it ourselves (i.e., within LIGO/LSC). This is still an open question.

In addition, we would like to switch to using a single EOM for all 3 frequencies of phase modulation. This technique has been demonstrated at LHO (SURF project under Dick Gustafson).

Connection to Advanced LIGO. This is a direct implementation of Advanced LIGO hardware.

5.2.2.   Pre-mode cleaner

It is not clear whether the existing pre-mode cleaners (PMC) could robustly handle 4-5× more power. There is currently an effort at LHO to make relatively minor changes to the existing design, reducing the amount of potentially contaminating materials, in the hopes of reducing optical losses and degradation of efficiency. The PMC design will be re-examined for Advanced LIGO, with a couple of potential changes being a longer cavity to support a larger beam size, and a vacuum, or inert-gas environment for the cavity. The R&D on the AdLIGO PMC is still at an early stage, and would need to be accelerated for such units to become available for middle LIGO.

Connection to Advanced LIGO. It would be desirable to implement an AdLIGO PMC for middle LIGO, to gain experience and test it under long-term exposure.

5.2.3. Faraday isolator

The current in-vacuum input Faraday isolator already shows thermal distortions, and on H2, the isolator was replaced with a design that partially solves these problems. But a better solution is needed for 30 W operation, and again we propose to implement the AdLIGO design for middle-LIGO. Compared to the initial LIGO design, the AdL Faraday incorporates (see Fig. 7):

- larger aperture TGG crystals, selected for low absorptance
- dual TGG crystals plus quartz rotator for birefringence compensation
- thermal lens compensation using a negative dn/dT material
- fused silica thin-film polarizers, instead of calcite polarizers

The only component that is still undergoing R&D for AdLIGO is the negative-dn/dT compensator, but the material that has been tested to date (KD*P) is perfectly adequate at 30 W. For AdLIGO, the negative-dn/dT element could be replaced *in situ* with a better element.
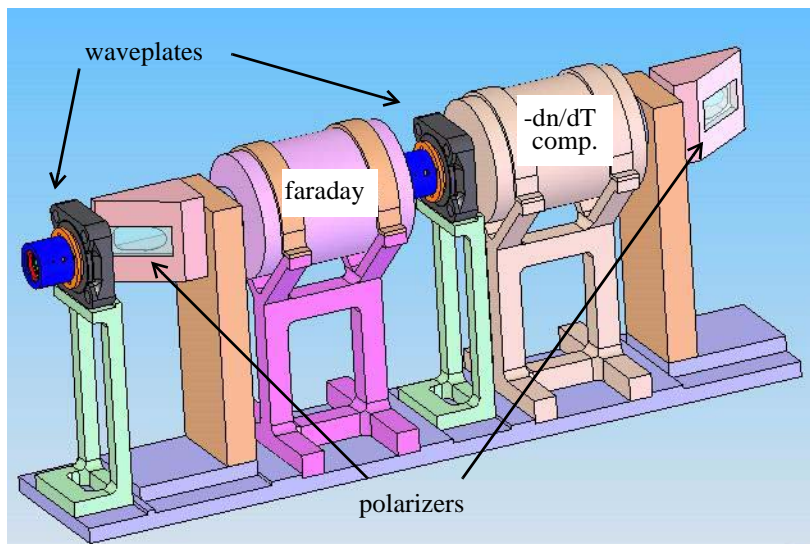

Figure 7: Current opto-mechanical design of the Advanced LIGO Faraday isolator.

Connection to Advanced LIGO. This is a direct implementation of Advanced LIGO hardware.

5.2.4. Higher quality optics (PSL & IO)

To reduce scattered light and ghost beams, we propose to replace off-the-shelf optics (lenses, mirrors, beamsplitters) in the PSL and IO beam lines with higher-quality, custom components. The replacement optics would have better anti-reflection coatings, and less scatter. A comprehensive collection of components would be purchased, which should also serve all or most of the needs of AdLIGO as well.

5.2.5. Mode cleaner mirror cleaning

The optical transmission efficiency of the L1 and H1 mode cleaners is not very high, around 70%, implying losses significantly higher (~10×) than expected. Given the recent reduction of loss achieved by cleaning H1's ITMY, we propose to clean *in-situ* the mode cleaner mirrors.

On L1, the mode matching of the beam into the interferometer appears to relatively poor, with approximately 10% of the carrier power being reflected on resonance. This needs further study, but if the high reflectivity is due to mode mismatch, this could be fixed by repositioning MMT2, during the same vent that the MC mirrors are cleaned and the new isolator is installed.

5.3. Output mode cleaner & detection table

The implementation of an output mode cleaner (OMC) is an integral part of the power increase program, for several reasons:

- an OMC greatly reduces the power that must be detected at the anti-symmetric output port; otherwise, quadrupling the number of photodetectors is not an attractive option
- an OMC reduces the sensitivity to some technical noise sources
- it implements several aspects of the AdLIGO design: in-vacuum, seismically isolated signal detection; output mode cleaner, with either RF detection (unlike AdL) or DC detection (as in AdL); the AdL HAM chamber seismic isolation (SEI) system (if possible)

The OMC concept presents two major design options: a long OMC, with individually suspended mirrors versus a shorter, monolithic cavity; RF/heterodyne versus DC/homodyne readout. Regarding the first option, we propose to pursue the short, monolithic design, as it is simpler to implement and coincides with the AdLIGO baseline design. Regarding the second option, we propose to design for both types of readout, and be prepared to implement both types. Technical comparisons between the readout types are made in App. A; see also Ref. [4]. Here we discuss the hardware implementation of the OMC and signal detection.

The main elements of the OMC and DARM signal detection are:

- the entire DARM channel signal path will be in-vacuum, with some amount of seismic isolation; this is motivated by past problems with acoustic noise affecting the signal detections components, especially with the in-air OMC tested on H1 in 2004
- the OMC, photodetectors, and associated opto-mechanical hardware will be mounted in the HAM6 chamber (HAM12 for H2)
- HAM6 will be isolated from the rest of the vacuum system with a SS plate inserted between HAM6 and the mode cleaner tube (spool B-5A); the plate will have a window for the AS port beam

NEW SEPARATION PLATE
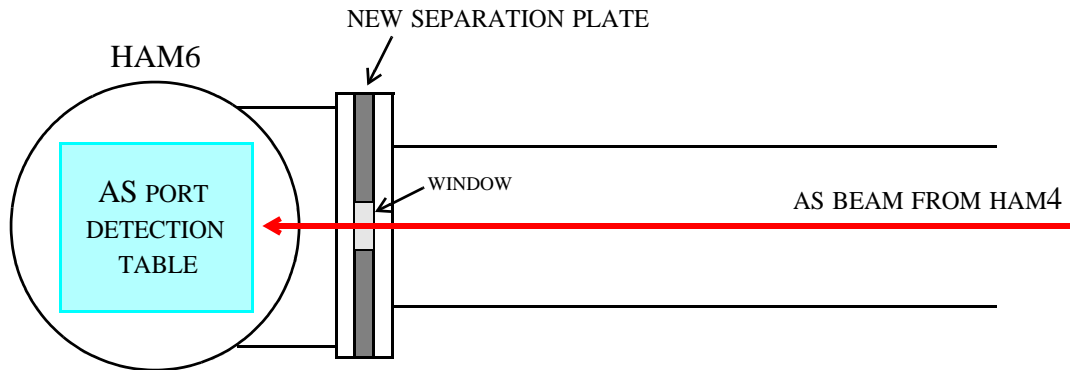
HAM6

AS PORT DETECTION TABLE

WINDOW

AS BEAM FROM HAM4

Figure 8: Sketch showing how HAM6 will be used for the AS port detection table. The AS beam will go through the beam reducing telescope and Faraday isolator on HAM4 as it does now, but then will be directed towards HAM6. A small fraction of the HAM4 beam will be directed out of HAM4 as it is now, for the WFS detection and other beam diagnostics. To make room for the vacuum separation plate (1.5" thick or so), the tube bellows at the HAM4 end will be compressed.

Separating HAM6 from the rest of the vacuum system (see Fig. 8) allows access to the detection table without having to vent additional volumes. Since the vacuum requirements for HAM6 are not very stringent (see below), this means that the recovery time from a HAM6 vent can be very short (less than a day).

Implementation of the OMC can also be considered on its own, independent of the laser power increase. In fact the strategy of starting with the OMC and then increasing the laser power has a lot of merit.

5.3.1. Detection table

Fig. 9 shows a simple block diagram of the detection table. It is conceptually very similar to the
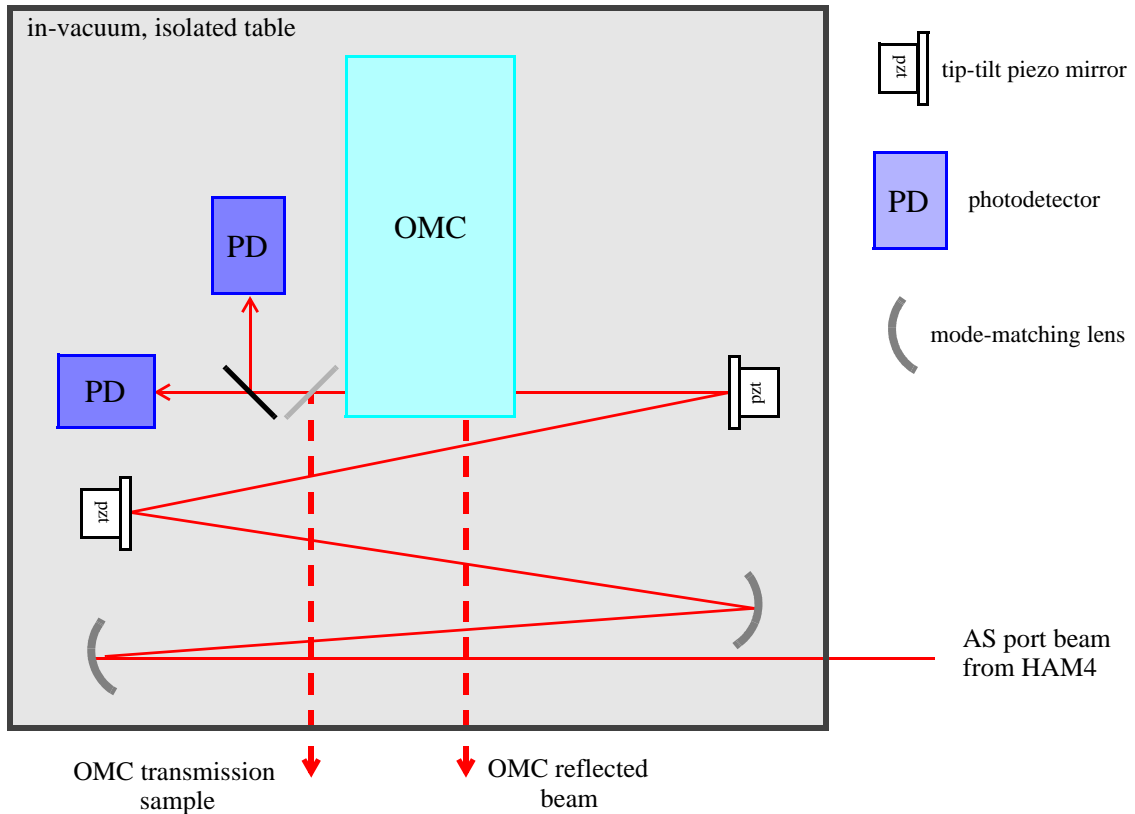
Figure 9: Conceptual block diagram of the in-vacuum AS port detection table. The OMC reflection beam, and a small fraction of the OMC transmission beam are brought out of the vacuum chamber for diagnostics.

detection table design for the 40m DC readout experiment. The mode-matching mirrors reduce the beam size from 4.5 mm radius to the OMC waist size, of order 0.5 mm radius. This mode-matching telescope can use the same design as the 40m DC readout experiment, using appropriate mirror radii-of-curvature; in this design, one of the MMT mirrors can be translated via a pzt, for remote mode-match adjustment.

5.3.2. OMC design and suspension

An OMC for RF readout would be relatively short (of order 10 cm round-trip path), and low finesse (30-100). The GEO600 OMC has such a design; see Ref. [4] for a description of its design, and a discussion of several design considerations for an OMC for RF readout. Testing of the GEO600 OMC on H1 showed that it was very sensitive to pointing fluctuations, and Keita Kawabe then pointed out that a 4-mirror OMC should be less sensitive than the 3-mirror design, due to its (2×) lower density of higher-order modes. Thus, an RF readout OMC would probably be a 4-mirror design, and Kawabe has worked out a geometry for such a cavity that uses spherical mirrors and minimizes astigmatism [6].

An OMC for DC readout would likely be longer (30-100 cm round trip) to support a larger beam size, and higher finesse (few hundred) to aggressively filter out RF sidebands and higher-order modes. The design details will be determined using the experience gained from the 40m DC readout experiment.

It is not clear whether the OMC will need additional vibration isolation, beyond that afforded by the isolated detection table. For RF readout, the maximum allowed length noise of the OMC, for its noise to be $10\times$ below the SRD, is $\sim 10^{-16}$ m/rtHz (for a particular choise of OMC parameters, see Ref. [4]). There are no good estimates at this time for DC readout. For Advanced LIGO, the baseline approach is to mount the OMC on a 6-DOF suspension isolator, having eigenfrequencies of order 1-2 Hz. This is likely in fact to be an isolated platform, on which the photodetectors are also mounted. If the design of the this isolator can be developed in the next 2 years, it would be desirable (and may be necessary) to implement it in middle-LIGO.

5.4. HAM6 detection table seismic isolation

The HAM6 detection table will need some level of seismic isolation. It is hard to know exactly how much is enough, but there are two main approaches, either of which is anticipated to work:

- make an initial LIGO-style passive isolation stack
- implement the Advanced LIGO HAM SEI system

The passive isolation stack would be the cheaper, simpler solution, and there are several options to this approach. One option is to reproduce exactly the current HAM stacks (HAM6 currently has none of the isolation stack components, only the piers exist). As a variant, the old-style viton 'cork' springs could be used, instead of the metal coil springs. They are better damped, and much easier to come by than the coil springs; they absorb more water, but that would not be an issue since the chamber would be isolated from the rest of the system. Another variant would be to support the stack from inside the HAM6 chamber, a potentially cheaper approach than reproducing the support tubes and bellows.

From the standpoint of AdLIGO, it would be preferable to implement the AdLIGO HAM SEI system, so that it could achieve the status of HEPI: a subsystem that has been installed and tested at the observatories, and only needs to be reproduced in AdLIGO. There are three design concepts that are under consideration for the AdLIGO HAMs:

- **baseline design:** a 2-stage, active system, which is essentially a slightly scaled-up version of the Stanford ETF prototype
- a single-stage active system; this would be cheaper and simpler than the 2-stage system, with less (but potentially adequate) isolation performance
- a single-stage passive isolation system, aka HAM SAS, as described in LIGO-G050267-00-R

The AdLIGO HAM isolation requirements are currently being reviewed, and the goal is to choose a design concept to develop in the fall of 2005.

5.5. Thermal distortion

Since we are proposing to increase the stored power in the interferometer by a factor of 4-5, the questions naturally arises: what about thermal distortions in the core optics? The experience with H1, prior to replacing ITMX, showed that, with the thermal compensation system, stable operation could be achieved in the presence of 100 mW of absorbed power in the ITM (the S4 case), but stable operation was elusive at twice that power level. If we take 100 mW as the maximum absorbed power, and assume that the ITMs absorb at the level typically seen in lab testing, we can arrive at a maximum beamsplitter power of:

$$P_{bs} < \frac{2 \times 100 \text{ mW}}{3.5 \text{ ppm/cm} \times 20\text{cm} + 0.8\text{ppm} \times 130} = 1.15 \text{ kW} .$$

With a recycling gain of 40, the maximum power incident on the recycling mirror would be 30 W, which is the target power level for middle-LIGO. Thus it appears feasible to operate at the proposed power level with the current thermal compensation system. Of course the installed optics may absorb more than this, and we may need to replace or clean *in situ* one or more optics.

6 SEISMIC NOISE MITIGATION

There are two motivations for improving the seismic noise isolation. The first is to reduce the seismic 'wall' frequency. The wall frequency is estimated to be 45 Hz (Fig. 3), higher than the SRD value of 40 Hz, and it could be as high as 50 Hz if other low-frequency noises are reduced. Second, reducing the rms motion (sub-10 Hz) could reduce non-linear conversion of such motion into the GW band.

6.1. PEPI at LHO

One idea would be to implement the PEPI system (Pzt-External Pre-Isolator) on the LHO test mass chambers. This is the isolation system that was installed at LLO prior to HEPI, and uses the PZT stack fine actuators and inertial sensors mounted on the stack cross beams, to give 2-DOF active isolation in the 1-3 Hz band.

To implement this at LHO, the fine actuators removed from L1 would be installed on the (4) ITM chambers of H1 and H2 (the ETM chambers already have fine actuators). Two low-noise inertial sensors would be needed per chamber, 16 total. On L1, GS-13 geophones were used. These are fairly expensive, roughly $8k each, but if purchased for this use they could be used later for the AdLIGO SEI systems. Another possibility could be to incorporate relatively cheap position sensors in the fine actuators, and use feed-forward from the existing STS-2 seismometers to achieve isolation.

The benefit of PEPI isolation at LHO would be (most likely) in reducing non-linearities from large, sub-GW band motions. An example is reducing fringe-wrapping noise from scattered light, a phenomenon that has been measured to exist now at LHO, at a non-negligible level.

6.2. External passive pre-isolation

Another concept is to add a simple elastomeric passive isolator to support the seismic cross beams (i.e., between the cross beams and HEPI at LLO, and between the cross beams and the piers at LHO). The idea is to add a well-damped resonance below 10 Hz in the horizontal plane, to provide passive isolation at ~10 Hz and above. The example isolator modeled for the 'Seismic (rubber)' curve of Fig. 3 moves the seismic wall frequency from 50 Hz down to 40 Hz. Clearly more analysis of the concept is needed; solutions could be tested on the LASTI BSC.

6.3. ISC detection table isolation

The interferometer detection chains are sensitive at some level to vibrations of their components (lenses, beamsplitters, photodetectors), due, e.g., to beam clipping or light scattering. While the anti-symmetric port length sensing chain in middle LIGO will be on a seismically isolated, in-vacuum platform, this still leaves the wavefront sensors and auxiliary degree-of-freedom length sensors vulnerable to the vibrations of the optics tables on which they are mounted. Though not a significant limitation at current sensitivity, the vibrational noise in these detection paths may become significant as the overall noise is reduced, and we may need to employ some vibration isolation for these optics tables. There are commercially available isolation systems that would most likely be adequate; for example, a pneumatic isolation system from TMC was tested on H2's ISCT10 in August 2005, and gave a factor of ~10 or more isolation from 10-100 Hz.

Connection to Advanced LIGO. Most of the detection chains in AdLIGO will be entirely in-vacuum, however there may be some cases where this is not feasible or desirable, and an isolated optics table would be needed.

7 SCATTERED LIGHT CONTROL

Below 100 Hz, the noise budget underestimates the measured interferometer noise, by up to a factor of 2-3. Scattered light is a potential source of the excess noise, and of course there are many possible scattered light paths. The original interferometer design called for light baffles in the beam tubes, installed at each end of the arm cavities, to block small-angle scattered light from the other end. These baffles have not been erected in the beam tubes. The end-station baffles may be erected during S5; if not, we would plan on erecting them after S5. The corner-station baffles need to be re-designed, to allow the TCS laser beams to pass through to the ITMs. New baffles should be designed and built to be ready at the end of S5.

8 SUSPENSION THERMAL NOISE REDUCTION

The main thrust of middle LIGO is to improve sensitivity in the shot noise limited region (above ~100 Hz) by increasing the laser power and improving the readout, but the frequency band below 100 Hz deserves some attention as well. In this region, between the shot-noise band and the seismic wall, the fundamental noise limit is suspension thermal noise. The expected thermal noise level of the existing test masses (suspension + internal) is already below the SRD noise target; Fig. 10 shows the ratio of the SRD noise to the predicted thermal noise, indicating the factor by

which the SRD could be improved upon, if shot noise were made negligible in this band and the thermal noise level were reached.
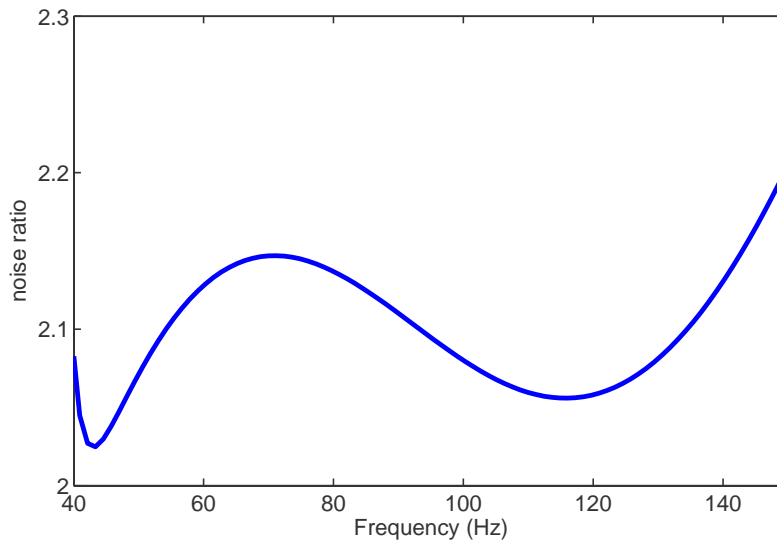

Figure 10: Ratio of the SRD noise curve to the predicted thermal noise (suspension + internal) for the existing initial LIGO test masses. Suspension thermal noise is calculated assuming a structure damping loss for the steel suspension wire of 3×10^{-4}, plus thermoelastic damping, and the laser beam centered on the optics (moving the beam down by 5-10mm could reduce the thermal noise below 100 Hz by about 20%). The internal thermal noise estimate uses a bulk material loss of 10^{-7}, and a coating loss of 2×10^{-4} and thicknesses of 3.9 µm (ITMs) and 7.7 µm (ETMs).

Possibilities for making reductions in the suspension thermal noise are discussed in Sec. 8.2. below. Significant modifications to the suspension mechanics are not being proposed, due to the cost, the downtime involved with significant in-vacuum work, and the non-AdLIGO R&D that would be involved (an example of a modification *not* being considered is a double-stage suspension).

8.1. Characterization of existing suspensions

The steel wire used in the initial LIGO suspensions is believed to have an internal (structure damping) loss of around 3×10^{-4}, and non-negligible thermoelastic damping, which exceeds structure damping above about 50 Hz (see Fig. 11). Measured Qs of the fundamental violin modes of the test mass suspension wires are typically around 150,000, though there is significant variation between suspensions, and even between different measurements on the same suspension. A Q of 150,000 implies a wire loss of 1.3×10^{-3}, close to the expected level from structure plus thermoelastic damping. A possible explanation for the lower observed Qs (~100,000) is recoil damping from modes of the suspension support structure, which would not affect the ~100 Hz thermal noise.

More work needs to be done to improve the thermal noise prediction for the existing suspensions. Specific measurements that would be useful are:

- measure the loss of the actual wire used in the suspension (i.e., a sample from the same spool), to determine the structure damping

- measure the Young's modulus of the suspension wire, references for which vary by about 20%, to improve the thermoelastic damping estimate
- measure the modal frequencies of the suspension support structure, to determine how recoil damping might affect violin mode Q measurements
- measure more suspension violin mode Qs, including those of higher harmonics

8.2. Suspension fiber improvements

Suspension thermal noise could be reduced by replacing the steel suspension wire with a lower loss fiber, within the existing suspension structure. Most simply, this would be done just by exchanging the wire loop by another wire loop of a different type. Another suggestion that has been made, in the context of introducing fused silica fibers, is to support the test mass in some sort of cradle, to which the new fiber would be attached. The challenge would be to design a cradle that fits in the suspension cage.

The thermoelastic damping loss of some potential suspension fibers is shown in Fig. 11. From this standpoint, steel ribbons and invar look like attractive options. Reference [6] gives experimental data on the loss of many of these materials. For invar, the loss data lies between $0.8\text{-}1.6\times10^{-4}$ in the 10-400 Hz band; the data are distributed in frequency without a discernible pattern, and could represent an upper limit rather than true material dissipation. Depending on the structure loss, steel ribbons or invar could offer a thermal noise reduction of sqrt(2)-2, in the 40-150 Hz band. The following R&D is suggested for alternative suspension fibers:

- measure the loss and strength of steel ribbons
- measure the loss and strength of invar, and super-invar
- investigate methods to suspend a test mass with a ribbon, so that flexible direction is along the optic axis
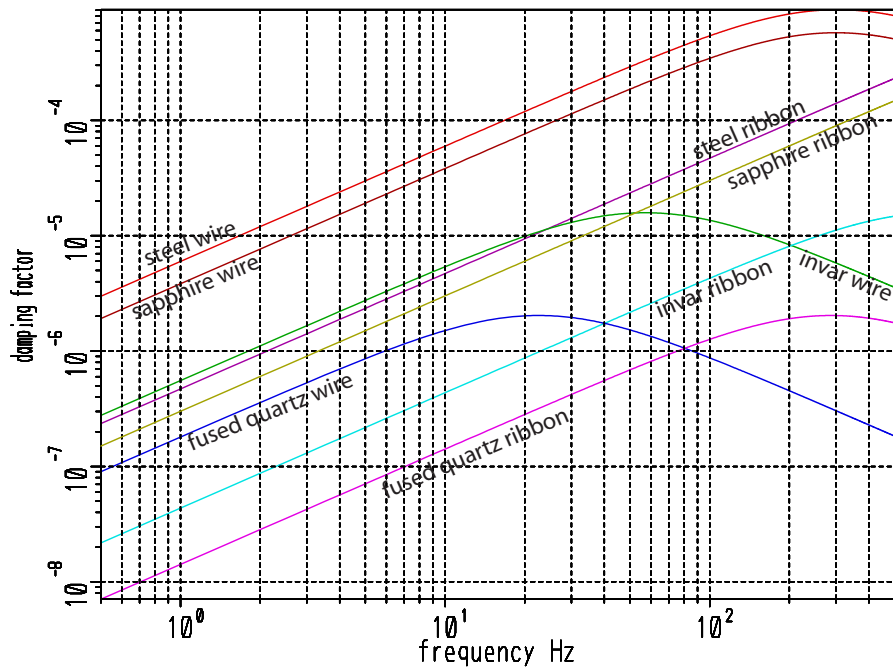
Figure 11: Thermoelastic damping factor for different suspension fiber shapes and materials; this does not include structure damping (or any other kind of damping). For each case, the test mass is supported by 2 fibers, each loaded to the stress level given in App. 2; the 'ribbons' are rectangular cross section fibers with a 10:1 aspect ratio.

9   IMPLEMENTATION STRATEGY

For the improvements outlined in Sec. 5, there are choices in how these are implemented: do we implement it all at once, or in stages? how is it staged across the interferometers? do we implement everything on all three interferometers, or just the 4km ones? which OMC and readout type (RF versus DC) do we try first? Here is one strategy to consider:

- Perform much of the vacuum work on all interferometers right after S5. This includes: installing new Faraday isolators; cleaning MC mirrors; any cleaning of core optics; installation of vacuum separation plate for the output HAM(6); installation of any new baffles. Duration: 1 month
- Install and commission the output mode cleaner and associated seismic isolation system in HAM6 of H1. Duration: 9 months
- Implement the laser power upgrade on L1. Gain experience with laser and operation of the interferometer with higher stored power (though the AS port detected power could not be significantly increased with the OMC). Duration: 6 months
- Then, the OMC could be implemented on L1 and the laser upgrade on H1, benefiting in each case from the experience gained at the other observatory. Around 18 months after the end of S5, all hardware upgrades could be made, and a significant amount of commissioning accomplished.

The roles of L1 and H1 in this scenario could be swapped. Any seismic isolation upgrades should be done in parallel with the above. This scenario does not address what we do with H2.

APPENDIX A   TECHNICAL NOISE REDUCTION

Middle LIGO noise budgets, including technical noise sources, are shown in Fig. 12, comparing the cases of RF and DC readout of the GW channel. The components of the noise budgets are described below.
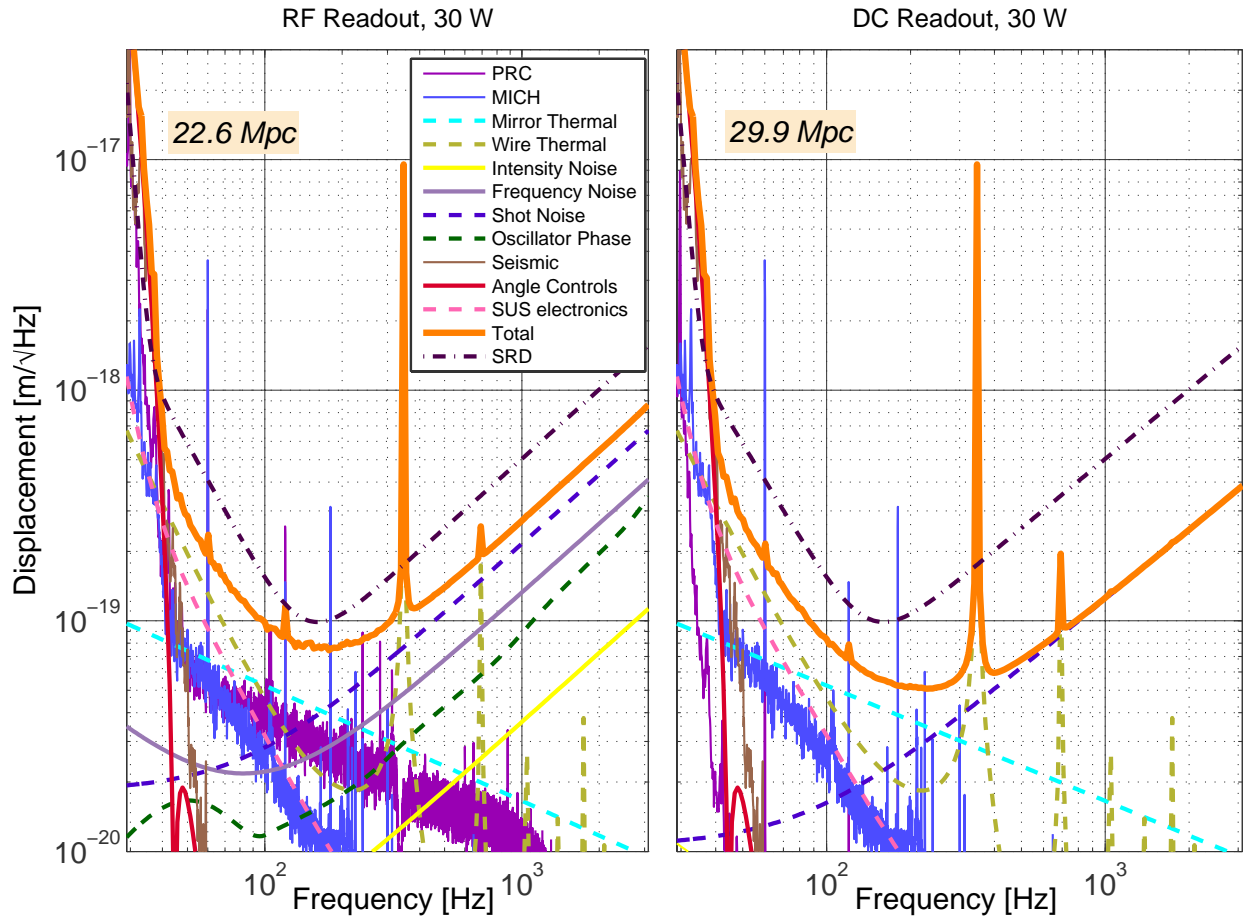

Figure 12: Middle LIGO noise budgets, including technical noises, comparing RF and DC readout of the GW channel. See text for explanation of noise components. The NS-NS inspiral range is given in the upper right corner of each panel, and can be compared to the range for the ideal case (negligible technical noise; i.e., the orange curve in Fig. 3) of 33 Mpc.

Shot Noise. The shot noise estimates assume the presence of an output mode cleaner, so that only the TEM_{00} component of the carrier light is transmitted to the detectors; the power in this component is 5×10^{-6} of the carrier beamsplitter power. For the RF readout, the shot noise is calculated with: a modulation depth of 0.25 (to maintain a high SNR for the auxiliary loops); RF sideband power transmission from the RM to the AS port of 60%; overlap of the RF sidebands with the arm

cavity mode of 70%. For the DC readout, the shot noise is calculated with an arm cavity differential offset of 20 pm, producing a AS port power of 200 mW (80 ma per photodetector).

Suspension (SUS) Electronics. This includes noise from the core optic bias modules and the main coil drivers. The curve has been calculated assuming the following set of improvements are made:

- Angle bias modules fixed so that they have an output voltage noise of 10 nV/rtHz, plus the thermal noise 15 kohm series bias resistors. To achieve such high resistor values, vacuum incursions will be required to tweak the alignment of some of the test masses with the PAMs (pitch adjustment magnet). In addition, higher voltage bias supplies would be used (300 V).
- The low-pass filtering on the PA-85 gain stage in the coil driver is increased by a factor of 2.
- The R-C-R filter at the output of the PA-85 gain stage is reduced by a factor of 2 (increasing the effective series resistance).
- The beamsplitter noise is reduced with a more aggressive dewhitening filter (one similar to the ETMs).

The second and third modifications leave the range-vs-frequency essentially the same for run mode, but would reduce the lock acquisition transient range by a factor of 2.

Angular Noise. This curve combines the angular control noises from the optical lever and wavefront-sensor (WFS) loops, using control noise data from H1. No improvement over present performance is assumed (or called for).

MICH & PRC Noise. The overall noise level of these components has been reduced by a sqrt(2), from an assumed factor of 2 increase in detected pick-off power. As of September 2005, the pick-off detectors have 50 ma of photocurrent at full laser power. Detecting 100 ma of photocurrent may require 2 photodetectors. The MICH noise curves use an intrinsic MICH-to-DARM coupling of 1/137, and a decoupling factor from the real-time correction path of 160. For RF readout, the PRC noise curve uses an intrinsic PRC-to-DARM coupling of 1/1000, and a decoupling factor from the real-time correction path of 3. With DC readout, the current coupling mechanism of PRC to DARM, via modulation of the RF sidebands, will be gone; presumably it will be replaced by some smaller, as yet unknown, coupling mechanism. As a placeholder, the PRC noise is reduced by a factor of 10 for the DC case.

Intensity Noise. With the output mode cleaner, the static DARM optical offset of ~1 pm will be greatly reduced, thereby reducing the linear coupling of laser intensity noise. The coupling will then be dominated by the rms fluctuations in DARM, which are ~ 0.1 pm. With DC readout and a 10 pm DARM offset, the coupling is higher than the RF readout case at low frequencies, but becomes insignificant above 100 Hz due to the coupled-cavity filtering of the carrier. The laser RIN for both cases is taken to be 3×10^{-8}, independent of frequency.

Frequency Noise. For RF readout, this is limited by the common mode loop sensing noise, taken to be 3×10^{-7} Hz/rtHz at DC. This is 3× lower than the current sensing noise on L1; the improvement is assumed to be achieved by using the non-resonant sideband photodetector, with ~10× more light. The coupling of the sensing (frequency) noise to DARM is through a 0.5% imbalance of the arm cavity reflectivities (as measured on L1). For DC readout, the sensing noise is assumed

to be reduced to the above level, and filtered by the 1 Hz double cavity pole. The coupling is through an arm cavity pole mismatch, taken to be 2 Hz (about 2%).

Oscillator Phase Noise. For RF readout, the oscillator phase noise coupling is based upon the transfer function of Oscillator Phase-to-DARM (GW channel), measured on H1 in September 2005. The magnitude of this transfer function is about 1.5×10^{-14} meters/radian at 100 Hz, with an approximately f^2 frequency dependence. An older transfer function from L1 has more structure in it, and in general the coupling is higher than for H1 by a factor of a few. Therefore, for the plot in Fig. 12, the Sept '05 H1 transfer function measurement is multiplied by a factor of 3. The oscillator phase noise spectrum that multiplies the transfer function corresponds to the specification for the Wenzel crystal oscillators with varactor tuning that are now in use for the main modulation frequencies (2×10^{-7} rad/rtHz at 100 Hz).

APPENDIX 2   FIBER MATERIALS

material	Young's modulus dynes/cm^2 ($\times 10^{12}$)	density gm/cm^3	tensile strength dynes/cm^2 ($\times 10^9$)	design stress dynes/cm^2 ($\times 10^9$)	poission ratio	specific heat erg/gmK ($\times 10^6$)	thermal conductivity erg/sec/cmK ($\times 10^6$)	expansion coeff. 1/K ($\times 10^{-6}$)
fused quartz	0.70	2.2	15	7.7	0.17	7.7	0.138	0.51
sapphire	3.4	3.98	21	7.0	0.29	7.5	3.7	5.8
boron	4.1	2.57	36	10				
steel (LIGO)	1.76	7.8	13.4	6.71		4.5	4.6	11
invar	1.46	8.0	7.07	6.6		5.0	1.0	1.7

Table 1: Fiber material properties for Zener damping at 300K. The *design stress* values are used in Fig. 11; *tensile strength* is the breaking stress. The *design stress* for fused quartz (silica) is the value for the AdLIGO suspension design.

APPENDIX 3   REFERENCES

1. B. Owen, *Detectability of periodic gravitational waves by initial interferometers,* to be published in the proceedings of the 2005 Amaldi conference; available now to the LSC through the LSC web site.

2. P. Nutzman et al., *Gravitational Waves from Extragalactic Inspiraling Binaries: Selection Effects and Expected Detection Rates,* Astrophys. J. 612 (2004) 364-374.

3. http://www.st.northropgrumman.com/ceolaser/, in particular the RB Plus line of laser modules.

4. R. Adhikari, *DC Readout in LIGO I,* LIGO-G050091.

5. P. Fritschel, *Output Mode Cleaner Design,* LIGO-T040018.

6. K. Kawabe, *Design and Performance of the Output Mode Cleaner,* LIGO-G040326-00-D.

7. G. Cagnoli, L. Gammaitoni, J. Kovalik, F. Marchesoni, M. Punturo, *Low-frequency internal friction in clamped-free thin wires,* Physics Letters A, 255 (1999) 230-235.

Appendix 4   Rough cost estimates for middle LIGO options

	Qty	unit cost, k$	total for 3 ifos, k$			Notes
Power Increase						
EO modulators	12	4	48			UFI estimate
Faraday isolators	4	25	100			UFI estimate
PSL/IO optics	1	100	100			Custom order to REO
Laser	4	185	740			LZH 4-rod ampilfier
Subtotal				988		
Output mode cleaner						
Vacuum: plate + HW	3	25	75			
OMC cavities	4	10	40			
OMC suspension	3	15	45			
Opto-mechanical HW	3	25	75			
Electronics	3	25	75			
Subtotal				310		
Seismic isolation options				delta		
passive stack	3	60	180		180	
HAM SAS	3	350	1050	870		
Active SEI (1 stage)	3	500	1500	1320		
Seismic isolation						
PEPI sensors	18	8	144			GS-13s; might not need this performance
PEPI control elects.	5	15	75			New PCIX HW at 5 stations; might instead be able to patch into existing HW at end stations
ISCT isolation	6	25	150			2 tables per IFO; Minus-K units, e.g.
External rubber pre-iso.	48	0.5	24			12 BSCs x 4 corners; guess on cost
Subtotal				393		
ITM beam tube baffles	4	7	28		28	use existing support frames

Total, w/ basic SEI	1899	
Total, w/ HAM SAS	2769	
Total, w/ active SEI	3219	